Moeck, I., Kwiatek, G., Zimmermann, G. (2009): Slip tendency analysis, fault reactivation potential and induced seismicity in a deep geothermal reservoir. - Journal of Structural Geology, 31, 10, 1174-1182

DOI: 10.1016/j.jsg.2009.06.012

# Slip tendency analysis, fault reactivation potential and induced seismicity in a deep geothermal reservoir

Inga Moeck*[1], Grzegorz Kwiatek[2] and Günter Zimmermann[1]

Helmholtz Centre Potsdam GFZ, [1]Section Reservoir Technologies, [2]Section Geomechanics and Rheology, Telegrafenberg, D-14473 Potsdam, Germany

*Corresponding author: E-mail address: moeck@gfz-potsdam.de, phone +493312881573, fax +493312881450

## ABSTRACT

A slip tendency analysis is used to assess the reactivation potential of shear and dilational fractures in a deep geothermal reservoir in the Northeast German Basin, based on the notion that slip on faults is controlled by the ratio of shear to normal stress acting on the plane of weakness in the in situ stress field. The reservoir rocks, composed of Lower Permian sandstones and volcanics, were stimulated by hydraulic fracturing. A surprisingly low microseismic activity was recorded with moment magnitudes $M_W$ ranging from -1.0 to -1.8. The slip tendency analysis suggests a critically stressed reservoir exists in the sandstones, whereas the volcanic rocks are less stressed. Rock failure first occurs with an additional pore pressure of 20 MPa. Presumed failure planes form a conjugate set and strike NW and NE. Slip failure is more likely than tensional failure in the volcanic rocks because high normal stresses prevent tensional failure. These results from slip tendency analysis are supported by the spatial distribution of recorded microseismicity. Source characteristics indicate slip rather than extension along presumed NE striking failure planes. This suggests that slip tendency analysis is an appropriate method that can be used to understand reservoir behavior under modified stress conditions.

Key words – Slip tendency, Enhanced Geothermal Systems, Hydraulic stimulation, Fractured reservoirs, Stress analysis, Seismicity

## 1. Introduction

A knowledge of the reactivation potential of faults is a critical issue in the development of man-made geothermal reservoirs, where hydraulic stimulation treatments are routinely applied to enhance permeability; the concomitant pore pressure increase also commonly induces seismicity. Such fracture initiation coupled with microseismic events is necessary to generate additional fractured flow paths that enhance permeability and hence productivity. However, a fluid injection which is not adjusted to the in situ stress field and rock strength conditions can lead to undesirable seismicity (Deichmann, 2008). The effects of stress field changes on fault kinematic behavior need to be understood, and fault reactivation potential should be estimated before stimulation treatment. In this study, we used a slip tendency analysis based on frictional constraints to assess the likelihood of fault reactivation in a stimulated geothermal reservoir.

Groß Schönebeck is the key site in the Enhanced Geothermal Systems (EGS) of the Northeast German Basin and was stimulated by hydraulic fracturing in 2007. A well doublet, with a production and an injection deep well is established at this site (Fig.1). The reservoir rock consists of red bed sandstone and andesitic volcanic rocks of Lower Permian age at roughly 4,200 m depth (Moeck et al., 2008). Regionally, the maximum horizontal stress in the Lower Permian subsalt successions trends NE in a normal faulting stress regime (Röckel and Lempp, 2003). The Northeast German Basin is a seismically quiet region, thus stress measurements originate from borehole data rather than from focal mechanisms (Heidbach et al., 2007). The site-specific stress field is known from hydraulic tests, borehole data analysis and stress ratio estimation (Moeck et al., 2008). An extensive stimulation treatment in the newer well

GrSk4/05 was carried out in both the volcanic and sedimentary successions (Zimmerman et al., 2008). To assess the seismic response of the reservoir to changing stress conditions resulting from the massive fluid injection, a seismic network, composed of a borehole geophone and additional surface stations, was installed in the off-set well GrSk3/90 (Fig. 1) and was used to record microseismic activity during and after stimulation of the volcanic rocks (Kwiatek et al., 2008) and sandstones.

Place here Fig. 1.

The principal aim of this paper is to test the likelihood of induced seismicity along fractures with certain orientations from the perspective of fault reactivation related to stress field perturbations. With the slip tendency analysis the potential for slip along any fault orientation with respect to the ambient stress field is investigated and therefore it is possible to assess the fault reactivation potential. This technique has been used for seismic-risk and fault-rupture-risk assessment in earthquake-prone areas (e.g. Morris et al., 1996; Collettini and Trippetta, 2007) and to understand the relative importance of shearing versus dilation behaviors along faults and bedding planes during deformation (Ferrill and Morris, 2003; Ferrill at al., 1998). In this paper we test the slip tendency method in its ability to forecast rupture plane orientation and intensity of rupture induced by hydraulic stimulation of geothermal reservoirs. To do this we calculate the shear and dilational stresses along mapped and suspected faults of the reservoir, evaluate slip and dilation potential, and compare the results with recorded and analysed microseismic events.

## 2. Slip and dilation tendency analysis

Slip tendency is the ratio of resolved shear stress to resolved normal stress on a surface (Morris et al., 1996). It is based on Amonton's law that governs fault reactivation:

$$\tau=\mu_s*\sigma_{neff} \quad (1)$$

where $\tau$ is the shear stress, $\sigma_{neff}$ the effective normal stress ($\sigma_n$ minus fluid pressure $P_f$), and $\mu_s$ the sliding friction coefficient (Byerlee, 1978). According to this law, stability or failure is determined by the ratio of shear stress to normal stress acting on the plane of weakness and is defined as the slip tendency $T_s$ (Lisle and Srivastava, 2004; Morris et al, 1996). Slip is likely to occur on a surface if resolved shear stress (the component of shear stress that is resolved in the direction of slip), $\tau$, equals or exceeds the frictional sliding resistance. Hence the slip tendency is given by:

$$T_s=\tau/\sigma_{neff} \geq \mu_s. \quad (2)$$

The shear and effective normal stress acting on a given plane depend on the orientation of the planes within the stress field that is defined by principal effective stresses: $\sigma_{1eff}=(\sigma_1-P_f) > \sigma_{2eff}=(\sigma_2-P_f) > \sigma_{3eff}=(\sigma_3-P_f)$ (Jaeger et al., 2007):

$$\sigma_{neff}=\sigma_{1eff}*l^2 + \sigma_{2eff}*m^2 + \sigma_{3eff}*n^2 \quad (3)$$

$$\tau=[(\sigma_1-\sigma_2)^2 l^2 m^2 + (\sigma_2-\sigma_3)^2 m^2 n^2 + (\sigma_3-\sigma_1)^2 l^2 n^2]^{1/2} \quad (4)$$

where l, m and n are the direction cosines of the plane's normal with respect to the principal stress axes, $\sigma_1$, $\sigma_2$ and $\sigma_3$, respectively. Eqs. (3) and (4) define effective normal stress and shear stress for compressional stress regimes, i.e. $\sigma_{1eff}$ is horizontal. Extensional and strike slip regimes can be derived by changing the order of the direction cosines in these equations (Ramsey and Lisle, 2000).

The dilation of faults and fractures is largely controlled by the resolved normal stress which is a function of the lithostatic and tectonic stresses, and fluid pressure. Based on eq. (3), the magnitude of normal stress can be computed for surfaces of all orientation within a known or suspected stress field. This normal stress can be normalized by comparison with the differential stress to give the dilation tendency, $T_d$, for a surface defined by:

$$T_d=(\sigma_1-\sigma_n) / (\sigma_1-\sigma_3) \qquad (5).$$

Slip and dilation tendency stereoplots are obtained by solving Eqs. (3) and (4) for all planes in 3D space, substituting in Eq. (2) for shear stress distribution along fault planes and by solving eq. (5) for normal stress distribution along fault planes, and plotting the results on equal area stereonets (Morris et al., 1996; Ferrill and Morris, 2003). This slip and dilation tendency analysis is a technique that permits rapid and easy visual assessment of stress states and related potential fault activity.

## 3. Slip and dilation tendency of the reservoir faults

The Groß Schönebeck multi-layered geothermal reservoir comprises Lower Permian red beds and volcanic (andesitic) rocks that form part of the infill of the Northeast German Basin. A slip tendency analysis for the Groß Schönebeck reservoir fault system was performed for both the Lower Permian (Rotliegend) red beds and the volcanic rocks using the in-situ stress values obtained from the red beds by Moeck et al. (2008) and from the volcanic rocks by Zimmermann et al. (2008). The following are known: the subsurface depths of the reservoirs (4.1 km deep for the sandstones and 4.2 km for the volcanics layer), the rock densities and thicknesses (Moeck et al., 2008), the vertical stress, $\sigma_V$, (100 MPa in the sandstones and 103 MPa in the volcanics). The average rock density of the overburden is 2.49 g/cm3 and is less than the commonly used value of 2.7 g/cm3, caused by the 1,300 m Upper Permian salt rocks

(2.1 g/cm3) which is typical for the Northeast German Basin (Moeck et al., 2008). The stress regime in the sandstone layer is known from site-specific borehole data as being transitional from normal to strike-slip faulting, indicated by a $\sigma_{Hmax}$~98 MPa, similar to the vertical stress, and a σhmin~55MPa. The value for $\sigma_{Hmax}$ is derived from borehole breakout analysis (Moeck et al., 2007), whereas the value for $\sigma_{hmin}$ is interpreted from hydraulically-induced minifracs carried out in both wells at the site. Minifracs are hydraulic tests that are used to induce small-scale artificial tensile fractures. The fracture opening pressure necessary to induce these fractures is similar to the minimum principal stress magnitude (Valley and Evans, 2007). In the volcanic layer, $\sigma_{Hmax}$ is assumed to be similar in value to $\sigma_V$, thus being 103 MPa or even higher due to the greater uniaxial compressive strength (UCS) of the volcanic rock. The $\sigma_{hmin}$ is known from a leak-off test and is 72 MPa. The hydrostatic pressure at 4.1 km depth is 43 MPa, and this is assumed to be appropriate for both reservoir intervals. Thus effective principal stresses would be: in the sandstone $\sigma_V=\sigma_{1eff}=57$ MPa, $\sigma_{Hmax}=\sigma_{2eff}=55$ MPa and $\sigma_{hmin}=\sigma_{3eff}=12$ MPa; and in the volcanic layer $\sigma_V=\sigma_{2eff}=60$ MPa, $\sigma_{Hmax}=\sigma_{1eff}=62$ MPa and $\sigma_{hmin}=\sigma_{3eff}=29$ MPa. The only stress value that is assumed and not analysed is the $\sigma_{Hmax}$ value in the volcanic layer. According to the frictional equilibrium that describes the limiting stress ratios for frictional sliding in the crust (Jaeger et al., 2007; Peska and Zoback, 1995), the stress value for $\sigma_{Hmax}$ can range between 100-140 MPa in this stress regime (Moeck et al., 2008; Moeck et al., 2009). We assume, however, that $\sigma_{Hmax}$ lies close in its value to $\sigma_V$, giving a similar stress ratio (R=0.06) in the volcanics to that in the sandstone layer (R=0.04). The orientation of $\sigma_{Hmax}$ is interpreted from hydraulic fractures in the sandstone layer, indicating an orientation of $\sigma_{Hmax}$=018.5°± 3.7° and implying a trend of $\sigma_{hmin}$ of 108.5°±3.7°.

Our analysis focuses on the conditions influencing the initiation of fault slip, meaning the point at which the slip tendency equals the frictional resistance to sliding. The Hoek-Brown classification of rock masses was used to estimate the strength parameters and thus different mechanical properties of sandstone and volcanic rock (Hoek, 1990) (Table 1). The applied parameters are the uniaxial compressive strength (UCS) of the intact rock and the constants s and m, which depend on the characteristics of the rock mass. The value s takes the disturbance of rock mass by fractures and weathering into account, whereas the value m reflects the geometrical shape of intact rock mass fragments. These constants can be taken for characteristic lithologies from the geological strength index (GSI), introduced by Hoek (1994). Sandstones are usually less competent rocks than most volcanic rocks. Effectively, the failure initiation and mode are therefore expected to differ in these two lithologies. The rock integrity (disturbance, grain size and shape) are taken from well bore investigations from offset wells. Accordingly, both the sandstones and the volcanic rocks are fractured and have a Hoek-Brown value of s=0.00198 (describing the rock mass quality), whereas the value m (describing the intergranular contact and grain size) varies between the sandstone (m=2.03) and the andesite (m=2.301). The UCS for the sandstone is $\sigma c$=79.3 MPa, and for the andesite, the UCS is $\sigma c$=101.5 MPa as determined by point-load tests on core samples (Moeck et al., 2009). These values for intact rock may be too high for reactivation analysis of faults which commonly have lower strengths than cohesive intact rock. The Hoek-Brown strength classification, however, considers a reduced rock strength produced by higher fracture density. In particular, we classified the volcanic rocks as being fairly intact masses based on analysis of core samples from the older well of the test site. The UCS used effectively allows for a reduced rock strength due to the presence of fractures. The values of rock strength parameters and characteristics of the in situ stress field used in the slip and dilation tendency analysis are summarized in Table 1.

Place here Table 1

The resulting slip tendency stereo plots show that in both the volcanic and the sandstone layers faults with a high slip tendency have tight bimodal or small-circle girdle distributions about $\sigma_3$ (Fig. 2A-B). This indicates that both normal and strike-slip faults can co-exist in the reservoir. Normal faults strike NE-SW and dip moderately (~50°) to the SE or NW. Strike-slip faults strike NE-SW and NW-SE as steeply dipping planes (>80° dip) (Fig. 2A). This analysis indicates that the maximum slip tendency developed in the sandstone interval is approximately 0.86 and in the volcanic interval it is approximately 0.39. These values imply that the sandstone interval is very close to a critical stress state, whereas the volcanic interval would require substantial additional pore pressure values to induce slip (Fig. 2D-E). A high dilation tendency is indicated in both the sandstone and volcanic rocks along steep NNE-SSW-striking fracture planes along which the normal stress is as low as the minimum principal stress (Fig. 2C). Extensional fractures are therefore expected along NNE-SSW sub-vertical planes. The stress difference ratios (Fig. 2F) show the reservoir rocks within the envelope of most realistic conditions for stress in the crust (Byerlee, 1978). The volcanic rocks lie in the lower portion of this envelope - indicating low slip tendency – whilst the sandstone layers lie in the upper portion of the envelope - indicating high slip tendency of optimally oriented faults.

### *3.1 Implications for fault-reactivation potential and induced seismicity*

Although the Northeast German Basin is not prone to earthquakes, it is important to know whether stimulation treatments could reactivate existing faults and cause unexpected seismicity. The slip tendency analysis indicates that the reactivation potential for any faults in the volcanic layer is very low. The maximum slip tendency is less than 0.5 and is well below the value of frictional strength of a rock mass at that reservoir depth (Fig. 2B). An additional pore pressure of 24.5 MPa would be necessary to increase the maximum slip tendency within the volcanic interval to about 0.8 (Fig. 2E). This would approach failure conditions for these rocks and would likely initiate slip along preferential fault planes. These preferential fault planes are NE-SW-striking, moderately dipping normal faults and steep NNW- and NNE-striking strike-slip faults (Fig. 2B). The large increase in pore pressure (over 24 MPa) required to generate slip within the volcanics implies that substantial induced seismicity during stimulation is unlikely.

Place here Fig. 2

## 4. Induced Seismicity

### *4.1 Stimulation experiment*

Three hydraulic treatments were performed in well GrSk4/05 during the summer of 2007. At the beginning of the stimulation campaign, leak-off tests carried out in both the volcanic and sandstone layers yield the fracture opening pressures, which are similar to the minimum horizontal stress magnitude. In the volcanic rocks, the minimum horizontal stress is $\sigma_{hmin}$~72 MPa. In the sandstone layer the minimum horizontal stress is $\sigma_{hmin}$~55 MPa. The difference in the stress magnitudes of layers that are vertically some tens of meters apart may reflect the competency contrast and different strength parameters in these two rock types. The volcanic rock is more competent and has higher strength values that potentially allows higher stress magnitudes.

The volcanic rocks were stimulated using a massive cyclic waterfrac treatment. A cyclic injection procedure was chosen because of technical constraints such as availability of fresh water and the expectation that a cyclic, high-flow rate injection (up to 150 l/s) would enhance fracture propagation and performance compared to a constant and low-flow (50 l/s) stimulation. This major injection was performed at 4,365 m MD (MD is the measured depth, i.e. the length of the well path), which corresponds to -4,175 m below sea level. The injection took place over a period of 6 days, between August 9th and August 14th, 2007 (Fig. 4). The resulting fracture dimensions were estimated using predictive fracture modeling, which yielded a fracture half length of up to 300 m (Zimmermann et al., 2008). A total volume of 13,170 $m^3$ of water was injected. The maximum injection bottom hole pressure, calculated from the monitored well head pressure, friction losses and flow rates during injection (Zimmermann et al., 2008; Legarth et al., 2005), was 86 MPa (43 MPa overpressure), whilst the first pressure drop indicating fracturing occurred at 63 MPa (20 MPa overpressure).

Subsequently, two stimulation treatments were carried out in the porous and permeable Lower Permian sandstone formations at depth intervals of 4,204 m to 4,208 m MD (-4,068 m to -4,070 m) and 4,122 m to 4,118 m MD (-4,009 m to -4,005m), respectively. Bridge plugs isolated the stimulated well sections hydraulically. 500 $m^3$ of a high viscous gel in conjunction with approximately 100 tons of high strength proppants (ceramic grains that keep the induced fracture open and transmissive) were injected in both sandstone treatments at maximum bottom hole pressures of about of 40 MPa and 30 MPa respectively (Zimmermann et al., 2008).

### *4.2 Seismic network*

The deployed seismic network consisted of seven three-component seismometers, including a downhole 3C seismometer (Geospace HS-1 geophone, natural frequency $F_N$=15 Hz, sampling rate $f_S$=1000 Hz) operated at 3,800 m depth in neighboring borehole GrSk3/90, 500 m from the injection point. The additional instruments were installed either at the surface or in shallow boreholes ~60 m deep (Marc Sercel L4-3C, $F_N$=1 HZ, $f_S$=200 Hz or SM6-B,

$F_N$ = 4.5 Hz, $f_S$=200 Hz, respectively), at about 3 km distance from the well head. The acquisition system worked in continuous mode and was used to capture the results from both the massive injections into the volcanic and sandstone deposits. Noise levels at the seismic sensors were sufficiently low prior to injection and during relatively low injection rates, whereas during high injection rates almost the entire frequency range was contaminated by the noise created by the water pumps. As a result, the recording conditions were significantly limited during periods of higher injection rates.

*4.3 Seismicity*

A total of 80 microearthquakes with moment magnitudes $M_W$ ranging from -1.0 to -1.8 were detected but only by the downhole geophone sensor. The high dominant frequency of recorded seismic events (>130 Hz), large source-receiver distances, and strong damping in the sedimentary environment (for details see Kwiatek et al., 2008) prevented the remaining sensors from recording the seismicity.

The seismicity during stimulation of the volcanic rocks displays a different spatial behavior with progressing time. A relatively large number of seismic events, hardly detectable even by the downhole sensor, occurred at the beginning of the massive injection into the volcanic rocks (Fig. 3, cluster A). The events, scattered in time and space, could not be precisely located because of unfavorable signal-to-noise conditions. However, the calculated distances from S-P onset times for some of the recorded events suggest that they may have occurred in the vicinity of the injection area. Two prominent seismic sequences (clusters B, C in Fig. 3), tightly clustered in time, occurred towards the end of the first injection into the volcanic rocks. They consisted of more than 20 and 9 events, respectively, and were detected after the sudden drop in injection rate and well head pressure. Sequence C is composed of two spatial groups: one located close to events from cluster B (C1) and a second located very close to the injection point (C2). Almost no seismicity was recorded during stimulation of the sandstone.

Place here Fig. 3

*4.4 Location*

Only 29 events from the seismic sequences were located using the polarization analysis (Plesǐnger et al., 1986) to estimate the direction of incoming waves (backazimuth and angle of incidence) and S-P onset time differences as a measure of the distance. We assumed an isotropic velocity model with $V_P$ and $V_S$ velocities based on core sample measurements (Trautwein and Huenges, 2005). The located events are shown in Figs. 4 and 5A. The distance between the seismometer and seismic sources is well constrained because of sharp P and S onsets in the radiated seismic energy. The primary uncertainties in this data are the result of uncertainties in the velocity model. The maximum error for backazimuth angles (±10º) is higher than that for the angle of incidence (±5º) and corresponds to the maximum horizontal and vertical errors of ±125 m and ±63 m for clusters B and C, respectively.

Events from clusters B and C are interpreted to originate from a planar structure approximately 700 m away from the seismometer and ca. 250 m from the injection area (Fig. 4). We fitted a plane surface to the location coordinates using the least-squares technique. The strike and dip of the resulting plane was found to be 017º (±10º) and 52º SE (±5º), respectively. Unfortunately, due to the limited number of stations we were not able to calculate fault plane solutions. However, we performed waveform correlation analysis and amplitude ratio comparisons to distinguish any consistencies between events that might suggest the similarity of their rupture process. It was found that almost all recorded waveforms from located events are very similar. Additionally, the spectral analysis performed on a subgroup of analyzed clusters made it possible to calculate the ratio between S and P energy released and other source characteristics, such as an approximation of static stress drop

(Kwiatek et al., 2008). The average $E_S/E_P$ equalled ~30, which is typical for a shearing type of focal mechanism, as suggested by Gibowicz & Kijko (1994). The calculation of static stress drop resulted in values oscillating around 1 MPa, which is a typical value for mining-induced seismic events (see Kwiatek et al., 2008 for a detailed analysis).

Place Fig. 4 here

## 5. Discussion

The processing of the analyzed microseismic events indicates an induced fracture plane with a strike and dip of 017º/52º SE. The fracture plane is consistent with an independent reinterpretation of geological data using 2D seismic profiles (Moeck et al., 2008). This investigation revealed a fault lying close to the interpreted plane (fault F28 in Fig. 5A) that strikes and dips similarly to the located planar cluster of seismicity. The recorded events possibly occurred along the existing fault plane. The fracture plane also agrees with the slip tendency plot of highly sheared fracture planes in the volcanic rock layer indicating a normal fault rather than a more steeply-dipping strike-slip fault (Fig. 5A). However, due to the limited number of sensors, we could not confirm by calculating the fault plane solutions whether the seismic events accommodated strike-slip or normal displacements. Nonetheless, we found recorded waveforms to be very similar, suggesting at least a common fault plane solution. Shearing rather than tension is indicated along the fracture plane by comparing the energy radiated from the P and S waves. This corresponds with a normal fault character, which is a shear plane with a normal slip vector (down the dip of the fault). Also, the static stress drop estimates are typical for a shearing type seismic event. Therefore, we suggest that the water stimulation of the volcanic rocks induced a normal fault rather than an extensional fracture plane.

The moment magnitudes of –1.0 to –1.8 during the microseismic events were surprisingly low for the massive water stimulation (with maximum additional bottom hole pressure of 43 MPa) into the volcanic rocks and less than first expected. The analysis of the slip tendency stereo plot and the Mohr-Coulomb diagram (Figs. 2B and 2E), however, reveals very low slip tendency; thus any faults in the volcanic rock and in that stress field are not susceptible to slip. Additionally, 24.5 MPa fluid pressures are necessary to increase the slip tendency from Ts~0.5 to Ts~0.8 along ideally oriented faults. The latter value, Ts~0.8, is a reasonable value for the coefficient of static friction under the crustal conditions of the studied reservoir at 4,200 m depth (Byerlee, 1978). It is therefore a limiting value where slip occurs, i.e. when the slip tendency equals or exceeds the frictional resistance of rock.

The calculated value of additional fluid pressure (24.5 MPa) needed to induce rock failure and weak micro-earthquakes is not exactly consistent with the recorded additional fluid pressure of 20 MPa (Zimmermann et al., 2008) during the stimulation. Figures 5B-C illustrate the ambient stress field and the modified stress conditions due to fluid stimulation in a Mohr circle diagram. The difference between the calculated and the measured additional fluid pressure to induce failure amounts to 4.5 MPa. Two reasons could account for this difference: (I) Error bounds on the input data need to be incorporated into the calculation. The UCS $\sigma c$ as determined by point-load tests has an error bound of 15 %, so the UCS is $\sigma c$=101.5±15 MPa, with a resulting error in the effective minimum horizontal stress of $\sigma_{3eff}$=9±3 MPa. The increase of the fluid pressure is calculated from the measured well head pressure, friction losses, and flow rates during stimulation and also does not have a quantified error bound. Figure 5B shows that the localized failure is likely when the error bounds of parameters $\sigma c$ and $\sigma_{3eff}$ are taken into account. (II) As stated above, the failure criterion used is the Hoek-

Brown criterion, which uses specified strength parameters and regards the intactness (which refers to the degree of fracturing) in the rock mass. In this study, the intactness was roughly estimated using core samples. The intactness of rock, however, has a strong influence on the compressive strength because a higher degree of fracturing causes a significant reduction in rock strength (Fig. 5C). The moderate quality type (m=2.301, s=0.00198, joint spacing 30-100 cm, UCS reduction to 14 MPa) used initially might not be appropriate for the intactness of the volcanic rock interval at depth (see Fig. 2E). In a poor quality rock mass (m=1.0870, s=0.00019, joint spacing 3-50 cm, UCS reduction to 6.8 MPa), failure would occur under the given stimulation conditions and measured fluid increase (Fig. 5C). The poor quality could relate to the close proximity of the reactivated fault.

The very low seismicity interpreted from the seismic events mirrors the low stress reservoir condition of the volcanic rock. In contrast, the sandstones are less competent and highly stressed as indicated by the presence of fault planes with high slip tendencies. We assume that critically stressed faults in the sandstones can be easily reactivated by additional fluid pressure during stimulation.  Low injection rates were used for the stimulation of the sandstones, resulting presumably in small fracturing and faulting events. Effectively, no significant seismicity was recorded during stimulation. Nevertheless, it is surprising that no microseismicity was recorded during stimulation of the sandstones. One reason could be the difference in the stimulation treatments. The volcanics were subjected to a large volume of injected water at high pressure, whereas the sandstones were treated with much smaller volume of gel plus proppants (ceramic grains) at lower pressures. Another reason could be a slightly different ambient stress field with a less critically stressed sandstone interval and higher critically stressed volcanic interval. However, the difference in the ambient stress states of both intervals remains and therefore it is more likely that the different stimulation treatments caused the difference in reactivation behavior. More comparisons of microseismicity and slip tendencies are necessary to understand and characterize the relationships between the locations of the microseismic events, increased fluid pressures, and stress state of fault segments. Slip tendency analysis in combination with rock strength parameters is a useful method to quantify the reactivation potential of faults. However, results from this method are more reliable if the stress field is well defined, e.g. by minifrac or leak-off tests performed prior to massive stimulation treatments.

Place here Fig. 5

## 6. Conclusions

Geothermal and hydrocarbon reservoirs are often stimulated by hydraulically-induced fractures to increase the productivity. Some geothermal systems especially require massive stimulation treatments to induce high flow rates of the geothermal fluid necessary for economic utilization. These engineered reservoirs called Enhanced Geothermal Systems (EGS) need to be investigated from a structural geological perspective to understand the fault and fracture patterns, stress states and fault reactivation potential. Particularly, the assessment of the fault reactivation potential is a crucial aspect prior to stimulation to mitigate undesired high seismicity and to best optimize the stimulation design.

In our case study from the Northeast German Basin, we applied the slip tendency method to characterize fault slip likelihood and slip directions in a geothermal reservoir in which a transitional stress regime is associated with both normal and strike-slip faulting. Results from the slip tendency analysis combined with geomechanical parameters show that faults in the volcanic succession of the reservoir have a low tendency to slip indicating that high additional fluid pressure is needed to reactivate potential strike-slip and/or normal faults. A massive water stimulation of the volcanic rocks over six days ended in a surprisingly low level of seismicity along a presumed normal fault, although the in situ fluid pressure was increased from 43 to 86 MPa through water injection in the well. First failure occurred with 20 MPa additional fluid pressure, whereas a required 24.5 MPa fluid overpressure was calculated using slip tendency for first failure. Although this difference may be explained by error bounds it could also indicate a high degree of fracturing in the volcanic rocks located near to the reactivated fault. The very low magnitude seismicity recorded during stimulation, however, is consistent with the results from slip tendency analysis. This study demonstrates that the slip tendency analysis, originally applied for earthquake assessment, provides an appropriate method to investigate, characterize, and understand the faulting behavior in engineered sub-surface reservoirs, such as Enhanced Geothermal Systems.

**Acknowledgements**

Alan Morris and an anonymous reviewer significantly improved the final form of this paper. We thank Alan Morris for his input to Figure 5 and additional constructive discussion, the editor Bob Holdsworth and Jim Faulds for helpful reviews and suggested improvements in this manuscript. The slip tendency analysis was carried out with the software 3DStress. The 3D geological model was developed with earthVision (DGI).

## References

Byerlee, J.D., 1978. Friction of rocks. Pure Applied Geophysics 116, 615-626.

Collettini, C., Trippetta, F., 2007. A slip tendency analysis to test mechanical and structural control on aftershock rupture planes. Earth & Planetary Letters 255, 402-413.

Deichmann, N., 2008. Seismicity induced by geothermal reservoir stimulation 5 km below the city of Basel, Switzerland. Proceedings, 3rd World Stress Map Conference, 15.-17. October 2008, Potsdam, Germany.

Ferrill, D.A., Morris, A.P., 2003. Dilational normal faults. Journal of Structural Geology 25, 183-196.

Ferrill, D.A., Morris, A.P., Jones, S.M., Stamatakos, J.A., 1998. Extensional layer-parallel shear and normal faulting. Journal of Structural Geology 20 (4), 355-362.

Gibowicz, S.J., Kijko, A., 1994. An Introduction to Mining Seismology. San Diego, Academic Press, 399p.

Heidbach, O., Fuchs, K., Müller, B., Reinecker, J., Sperner, B., Tingay, M., Wenzel, F., 2007. The World Stress Map, Episodes, 30 (3), 197-201.

Hoek, E., 1994. Strength of rock and rock masses. ISRM News Journal 2 (2), 4-16.

Hoek, E., 1990. Estimating Mohr-Coulomb friction and cohesion values from Hoek-Brown failure criterion. International Journal of Rock Mechanics 27, 227-229.

Hoek, E., Brown, E.T., 1988. The Hoek-Brown Failure Criterion-A 1988 Update. Proceedings of the 15th Canadian Rock Mechanics Symposium (Toronto, Canada), 31-38.

Jaeger, J.C., Cook, N.G.W., Zimmermann, R.W. 2007. Fundamentals of Rock Mechanics. 4th Edition, Blackwell Publishing, Oxford, UK

Kwiatek, G., Bohnhoff, M., Dresen, G., Schulze, A., Schulte, T., Zimmermann, G., Huenges, E., 2008. Microseismic event analysis in conjunction with stimulation treatments at the geothermal research well GtGrSk4/05 in Groß Schönebeck/Germany. 33rd Stanford Workshop on Geothermal Reservoir Engineering (Stanford, USA 2008), CD-ROM.

Legarth, B., Huenges, E., Zimmermann, G., 2005. Hydraulic Fracturing in Sedimentary Geothermal Reservoirs. International Journal of Rock Mechanics and Mining Sciences, 42 (7-8), 1028-1041.

Lisle, R.J., Srivastava, D.C., 2004. Test of the frictional reactivation theory for faults and validity of fault-slip analysis. Geology 32 (7), 569-572.

Moeck, I., Kwiatek, G., Zimmermann, G., Backers, T., Huenges, E., 2009. Assessment of fault reactivation potential in a deep geothermal reservoir of the NE German Basin (Germany). Geothermal Resources Council Transactions 33, in press.

Moeck, I., Schandelmeier, H., Holl, H.G., 2008. The stress regime of a Rotliegend reservoir of the Northeast German Basin. International Journal of Earth Sciences, DOI 10.1007/s00531-008-0316-1.

Moeck, I., Backers, T., Schandelmeier, H. 2007. Assessment of mechanical wellbore assessment by numerical analysis of fracture growth. EAGE 69th Conference and Exhibition, 11-14 June 2007, extended abstracts volume, D047, London, UK.

Morris, A., Ferrill, D.A., Henderson, D.B., 1996. Slip tendency analysis and fault reactivation. Geology 24 (3), 275-278.

Peška, P., Zoback, M.D., 1995. Compressive and tensile failure of inclined well bores and determination of in situ stress and rock strength. Journal of Geophysical Research, 100 (B7), 12,791-12,811

Plesǐnger, A., Hellweg, M., Seidl, D., 1986. Interactive high-resolution polarization analysis of broadband seismograms. Journal of Geophysics 59, 129-139.

Ramsay, J.G, Lisle R.J., 2000. Modern Structural Geology, Volume 3: Applications of Continuum Mechanics in Structural Geology. Academic Press, London 560p.

Röckel, T., Lempp, C., 2003. Der Spannungszustand im Norddeutschen Becken. Erdöl Erdgas Kohle, 119 (2), 73-80.

Trautwein, U., Huenges, E., 2005. Poroelastic behavior of physical properties in Rotliegend sandstones under uniaxial strain. International Journal of Rock Mechanics and Mining Sciences 42, 924-932.

Valley, B., Evans, K.F., 2007. Stress state at Soultz-sous-Forêts to 5 km depth from wellbore failure and hydraulic observations. Proceedings of the 32nd Workshop on Geothermal Reservoir Engineering. January 22-24. Stanford University, Stanford, CA.

Zimmermann, G., Reinicke, A., Brandt, W., Blöcher, G., Milsch, H., Holl, H.-G., Moeck, I., Schulte, T., Saadat, A., Huenges, E., 2008. Results of stimulation treatments at the geothermal research wells in Groß Schönebeck/Germany. Proceedings of the 33rd Workshop on Geothermal Reservoir Engineering. January 28-30, Stanford University, Stanford, CA.

Figure Captions

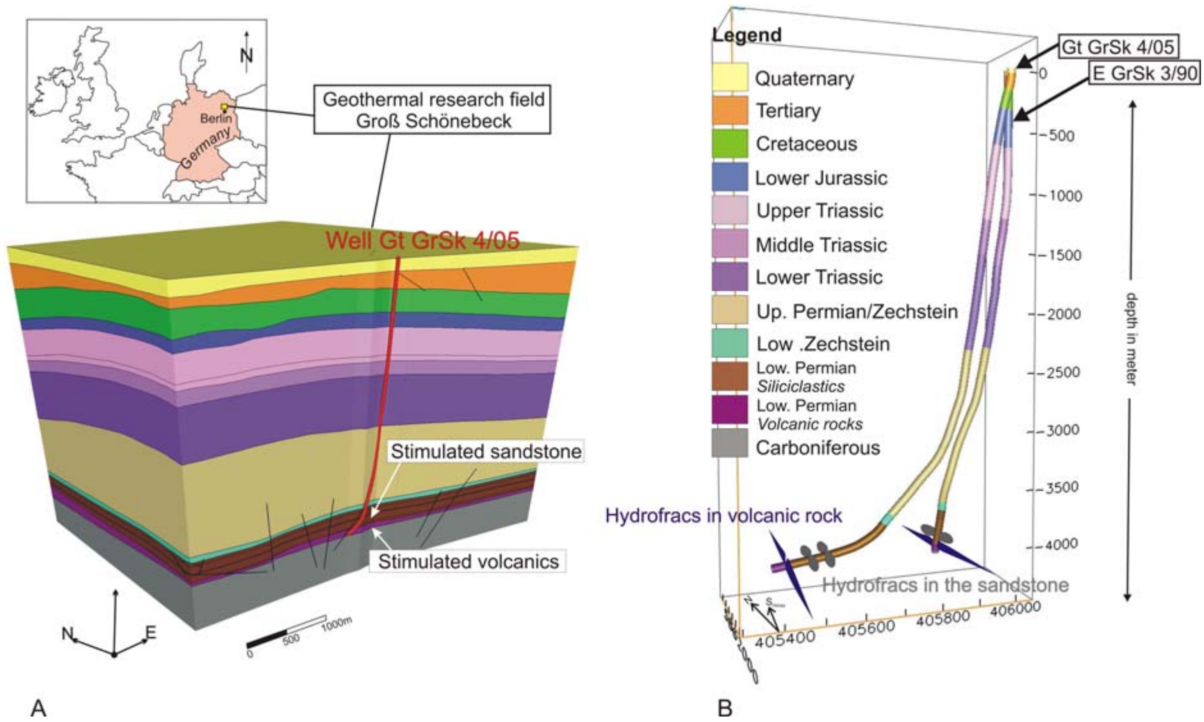


**Fig. 1.** (A) 3D geological model of the geothermal research field at Groß Schönebeck. The geothermal reservoir, consisting of siliciclastic and volcanic rocks, lies at 4,000-4,250 m depth. The red tube represents the hydraulically stimulated well. (B) Well doublet system with schematic illustration of hydraulically-induced fractures oriented along the maximum horizontal stress.

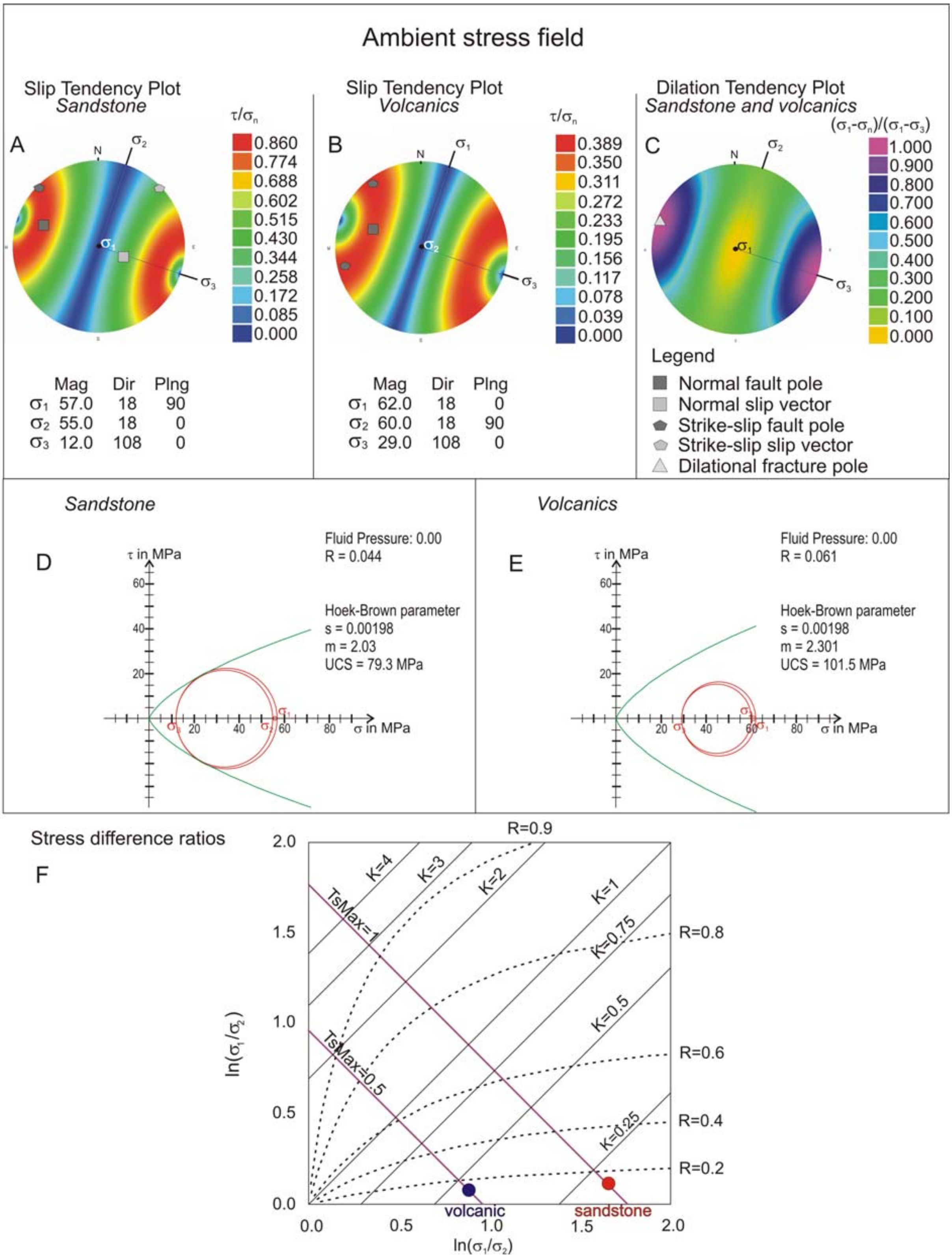


**Fig. 2. (A)** Slip tendency stereo plot of Lower Permian sandstones. (B) Slip tendency stereo plot of Lower Permian volcanic rocks. The plots show that both strike-slip and normal faulting could occur contemporaneously in the same stress field. (C) Dilation tendency plot of

both sandstone and volcanic rocks. Dilational faults would be subvertical with NNE strike. Tensional failure, however, is unlikely in the reservoir depth (4.0-4.2 km) due to high differential stresses. Shear failure is more reasonable as shown in the Mohr diagrams. (D) Mohr circle diagram illustrating stress conditions in the sandstone. (E) Mohr circle diagram illustrating stress conditions in the volcanics. (F) Stress difference ratio graph. K = $(\sigma_1/\sigma_2)/(\sigma_2/\sigma_3)$ and R =$(\sigma_1-\sigma_2)/(\sigma_1-\sigma_3)$ are stress difference ratios, Tsmax is the maximum slip tendency possible in the Earth's crust. The 0.5 and 1.0 contours of Tsmax envelop the most likely conditions of stress in the crust (Byerlee, 1978). The volcanic rocks are in the lower portion, the sandstone layers in the upper portion of this envelope.

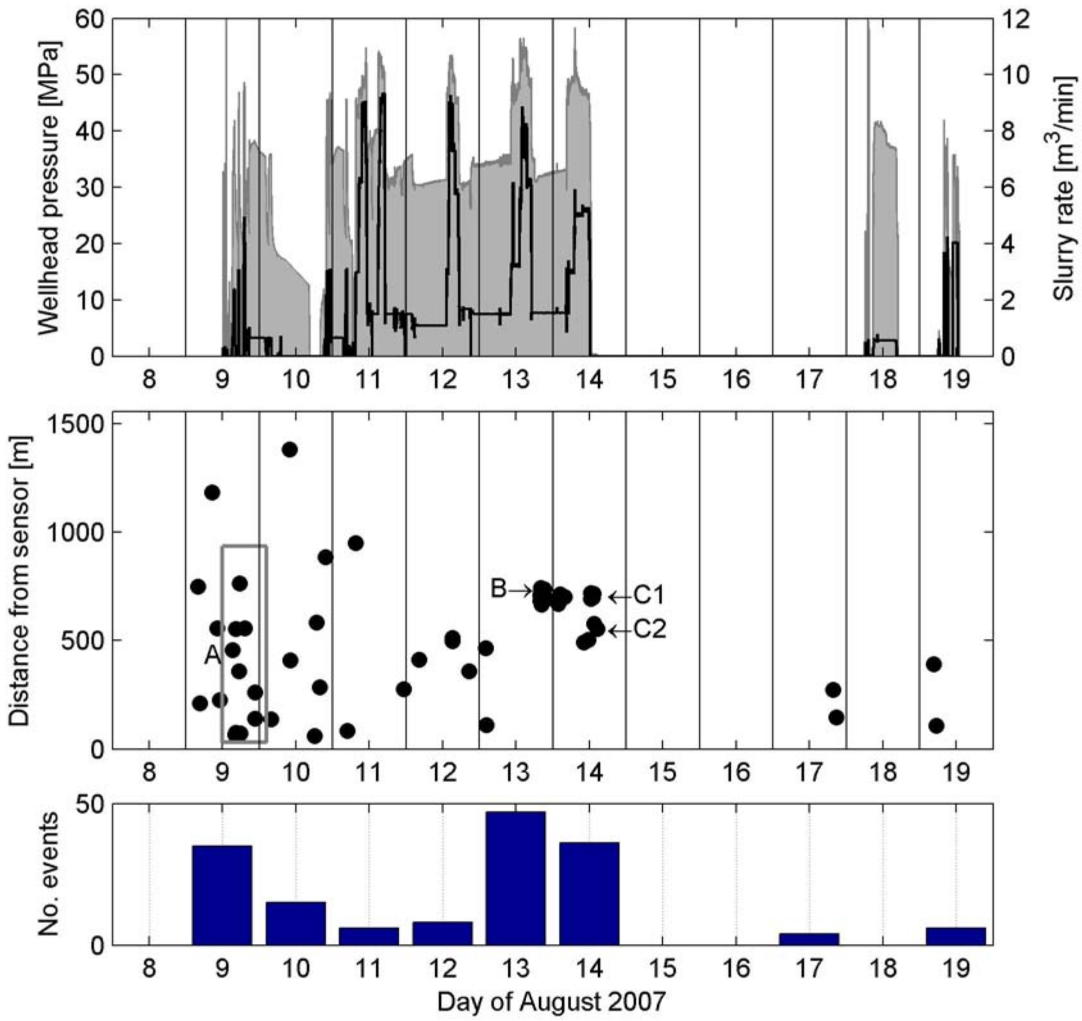


**Fig. 3.** Top panel: Well-head pressure (shaded area) and injection rate (black line) during the major (Aug 9-14) and minor (Aug 18-19) injection experiments carried out in the volcanic rocks and sandstones, respectively. Central panel: Distances between sensor and seismic events calculated from S-P times. The arrows and rectangle mark the A, B and C clusters. Bottom panel: Daily rate of detected seismic events. The drop in the number of seismic events between 10th and 12th of August may be partially related to the strong noise coming from water pumps.

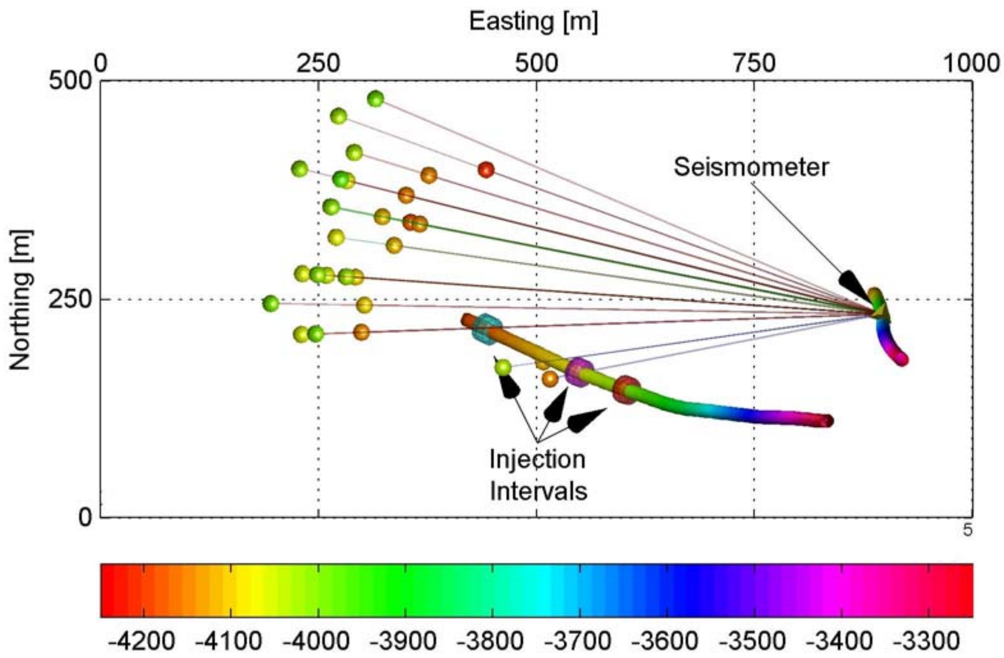


**Fig. 4.** Map view of the distribution of induced seismic events at the Groß Schönebeck geothermal site as determined from three-component recordings of the deep borehole seismometer. Color reflects the hypocentral depth of events plotted in accordance with the borehole trajectory for comparison. Semi-transparent fans denote maximum horizontal error as discussed in the text. The injection intervals in the volcanics (cyan ring) and sandstones (red, magenta rings) are also shown.

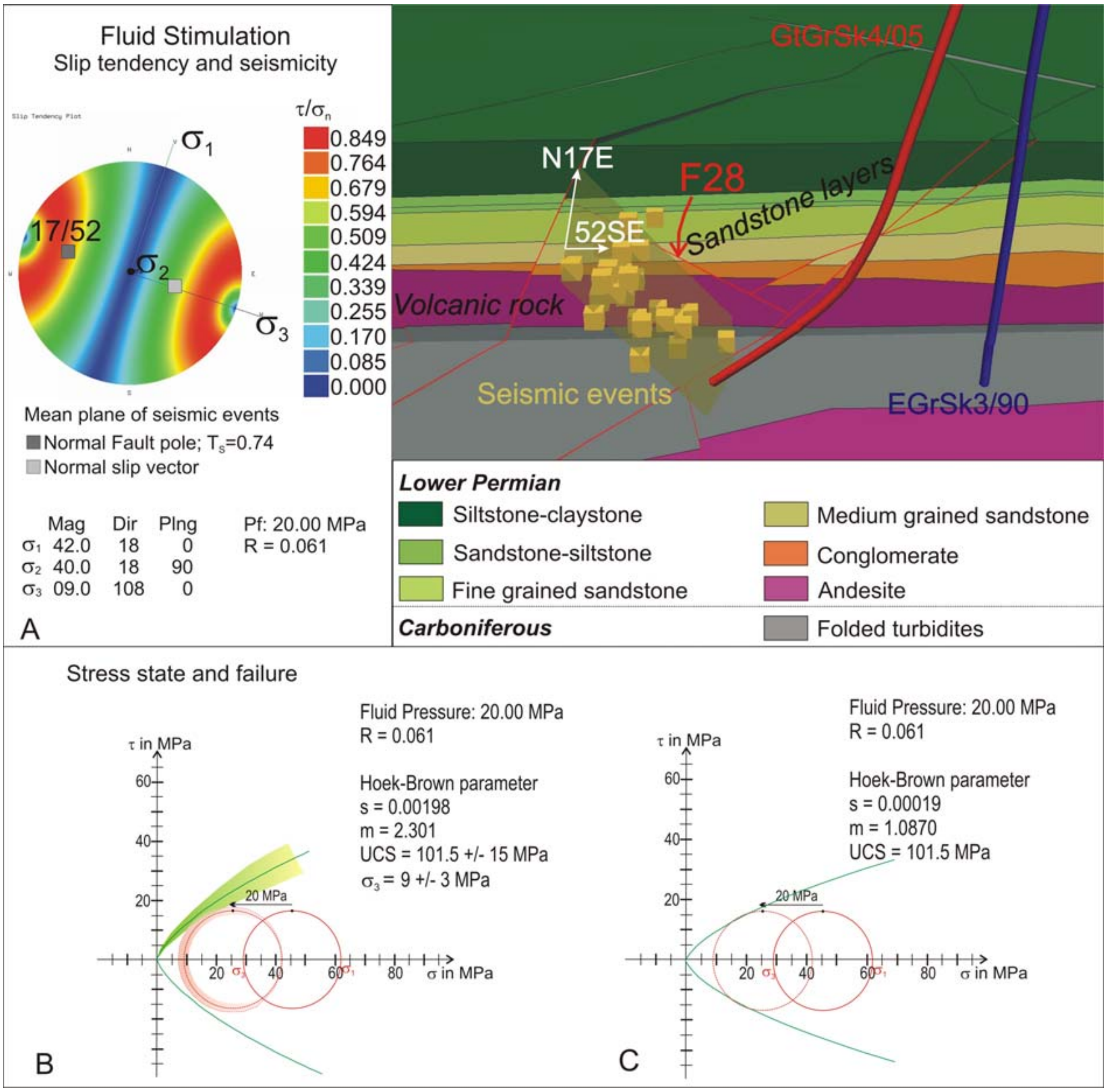


**Fig. 5.** (A) The slip tendency for the mean plane of the recorded seismic events (left), the spatial distribution of recorded seismicity (yellow boxes) and the least-square fitted plane (transparent yellow) (right). The distribution of seismicity fits the orientation of the F28 fault plane. (B) and (C) Fault reactivation due to fluid pressure increase during stimulation explained by Mohr circle diagrams. (B) Failure in a relatively intact rock mass (joint spacing 30-100cm) with the error bounds of UCS σc and $\sigma_{3eff}$. The hatched field represents the failure zone. (C) Failure in a poorly intact rock (joint spacing 3-50 cm). The higher degree of

fracturing could be explained by the proximity of a fault (fault F28) or by a generally higher degree of fracturing in the volcanics compared with the sandstone.

Table

**Table 1**

Relationship between rock mass quality and material constants in the updated Hoek-Brown failure criterion (From Hoek and Brown, 1988), and summary of in situ stress field characteristics

| **Empirical failure criterion**<br>$\sigma_1=\sigma_3+(m\sigma_c\sigma_3+s\sigma_c^2)^{1/2}$<br>$\sigma_1$= major principle effective stress<br>$\sigma_3$= minor principle effective stress<br>$\sigma_c$= uniaxial compressive strength of intact rock<br>m and s = empirical constants | ARENACEOUS ROCKS WITH STRONG CRYSTALS AND POORLY DEVELOPED CLEAVAGE<br><br>sandstone | FINE GRAINED POLYMINERALLIC IGNEOUS CRYSTALLINE ROCKS<br><br>andesite |
|---|---|---|
| FAIR QUALITY ROCK MASS<br>Several sets of moderately weathered/altered joints spaced at 0.3 to 1m<br>m<br>s<br>$\sigma_c$ | <br>2.030<br>0.00198<br>79.3 MPa | <br>2.301<br>0.00198<br>101.5 MPa |
| IN SITU STRESS FIELD | | |
| $S_V$ ($S_{Veff}$) | 100 (57) MPa | 103 (60) MPa |
| $S_{Hmax}$ ($S_{Hmaxeff}$) | 98 (55) MPa | 105 (62) MPa |
| $S_{hmin}$ ($S_{hmineff}$) | 55 (12) MPa | 72 (29) MPa |
| STRESS ORIENTATION | | |
| $S_{Hmax}$ | 18.5°± 3.7° | |
| $S_{hmin}$ | 108.5°± 3.7° | |